JOURNAL OF GEOPHYSICAL RESEARCH, VOL. 102, NO. E5, PAGES 10,889-10,903, MAY 25, 1997

Radar and photoclinometric studies of wrinkle ridges on Mars

Thomas R. Watters

Center for Earth and Planetary Studies, National Air and Space Museum, Smithsonian Institution Washington, D.C.

Mark S. Robinson[1]

U. S. Geological Survey, Flagstaff, Arizona

Abstract. Earth-based radar altimetry and image derived photoclinometric profiles were analyzed to examine both the long- and short-wavelength topography associated with wrinkle ridges on Mars. Photoclinometrically derived elevation data across wrinkle ridges were evaluated to determine the sensitivity of profiles to two empirical photoclinometric parameters, the horizontal digital number (HDN) and the scattered light value (SLV). The photoclinometric profiles are extremely sensitive to small variations in HDN. The sense of slope of a profile can be completely reversed over a range in HDN of as little as ±1. Comparably small variations in the SLV have relatively minor effects on the photoclinometrically derived elevations. The existence of elevation offsets from one side of the ridge to the other, reported in previous photoclinometric studies of martian wrinkles, were not confirmed through photoclinometry. In addition, no evidence of elevation offsets were found in Earth-based radar altimetry profiles across wrinkle ridges. In order to more accurately model wrinkle ridge topography, we controlled photoclinometrically derived elevations with long-wavelength topography obtained from the radar altimetry. The results of this study do not support kinematic models for the origin of planetary wrinkle ridges that involve deeply rooted thrust faults which separate crustal blocks at different elevations. A kinematic model involving buckling of shallow crustal layers into concentric folds that close, leading to the development of thrust faults, is consistent with wrinkle ridge morphology and terrestrial analogs. Recent geophysical studies of terrestrial analogs and the influence of shallow subsurface structures, particularly buried craters, on the localization of many wrinkle ridges on Mars suggest that thrust faults associated with the ridges are confined to the ridged plains material and do not extend into the lithosphere.

Introduction

The absence of high-resolution topographic data for Mars has hindered detailed morphologic studies, particularly of moderate and small-scale landforms on the planet. The extraction of elevation data from Earth-based radar observations and Viking Orbiter images using photoclinometry and stereogrammetry is critical to advancing our understanding of many of the geologic and tectonic processes operating on Mars. Earth-based radar altimetry profiles of Mars provide data on long-wavelength topography [Roth et al., 1980; Downs et al., 1982; Simpson et al., 1993], while short-wavelength topography can be derived from photoclinometry. A variety of landforms on Mars have been characterized using photoclinometrically derived topography [Wildey, 1975; Blasius et al., 1982; Howard et al., 1982; Davis and Soderblom, 1984; Pike and Davis, 1984; Tanaka and Davis, 1988, Herkenhoff and Murray, 1990; Golombek et al., 1991; Jankowski and Squyres, 1991; Mouginis-Mark and Robinson, 1992; Plescia, 1993]. Topography along a selected profile is determined by comparing brightness variations between adjacent pixels. It is assumed that all variation in brightness is due to varying topography, rather than albedo. The slope of the surface can be recovered by this method using a function that describes the photometric properties of the surface [Davis and Soderblom, 1984; McEwen, 1991]. Based on a study of wrinkle ridges in Lunae Planum and Arcadia Planitia, Golombek et al. [1991] and Plescia [1991, 1993] have concluded that elevation offsets from one side of a wrinkle ridge to the other observed in photoclinometrically derived profiles are structural in origin. However, the effect of minor variations in the photoclinometric parameters on the topographic profiles was not analyzed. In this study, Earth-based radar altimetry and photoclinometrically derived elevations are used to examine both the long and short wavelength topography associated with wrinkle ridges on Mars. To improve upon earlier work we evaluate the sensitivity of elevation data across wrinkle ridges derived through photoclinometry to small variations in two empirically derived parameters, the horizontal digital number (HDN) and the scattered light value (SLV). Implications for kinematic models for the origin of wrinkle ridges, estimates of horizontal shortening, and the nature and depth of thrust faulting are discussed.

[1]Now at Department of Geological Sciences, Northwestern University, Evanston, Illinois.

Paper number 97JE00411.
0148-0227/97/97JE-00411$09.00

Background

Photoclinometry

Photoclinometry is a useful technique for deriving topographic data for relatively small landforms with gentle slopes, because the spatial resolution of the extracted topography is only limited by the spatial resolution of the image and because the method is sensitive to small changes in slope [Davis and Soderblom, 1984]. In this investigation, elevation profiles were obtained using the asymmetric method developed by Davis and Soderblom [1984] coded in a module (TVPROF) incorporated into the Planetary Image and Cartography System (PICS). The Minnaert photometric function was used because it has been shown to be well suited for the surface of Mars [Binder and Jones, 1972; Thorpe, 1973; Davis and Soderblom, 1984; Tanaka and Davis, 1988]. The Minnaert function is defined by

$$B = B_0 \cos^k(i) \cos^{k-1}(e) \quad (1)$$

where B is the brightness number, B_0 is the surface normal albedo, i is the solar incidence angle, e is the spacecraft emission angle, and k is the Minnaert coefficient. Values for the wavelength-dependent Minnaert coefficient were derived by Tanaka and Davis [1988] for the Viking clear and minus-blue filters and by Thorpe [1973] for the red filter. Values for the violet, blue, and green Viking filters have not been published.

Two other key parameters in the asymmetric method are the SLV and the HDN. The SLV (sometimes referred to as the haze value), which corrects for light scattered in the atmosphere and from the surfaces outside the pixel area, is empirically chosen [Davis and Soderblom, 1984] by examination of shadowed regions within a frame [Tanaka and Davis, 1988]. A significant error in the estimated SLV will introduce vertical exaggeration into the derived profiles, and thus slopes will be inaccurate. A number of factors may contribute to variations in the SLV, including changes in albedo of the surface within a shadow, distance from a reflective surface, atmospheric variability, and calibration errors. Errors in the Viking Orbiter dark current correction may also contribute error in shadow values. The accuracy of the dark current correction is estimated to be approximately 1% for most of the Viking Orbiter images but can be up to 10% (U.S. Geological Survey, 1990, p. 3-3). The accuracy of the estimated SLV can be checked by comparing photoclinometrically derived elevations of a feature with elevations determined by shadow measurements, particularly when an image with a large incidence angle (as measured from the zenith) is available [Tanaka and Davis, 1988; Robinson, 1991].

The HDN (sometimes referred to as the flat field value) is a critical parameter in the asymmetric method [see Davis and Soderblom, 1984]. It is simply the brightness value of a horizontal surface in an image. Selecting a surface that is horizontal, based solely on photointerpretation, is subjective and errors in estimating the HDN can have a significant effect on the extracted topography. Large distortions in photoclinometrically derived profiles, including reversals in the true sense of slope due to misestimations in HDN, have been reported [Davis and Soderblom, 1984; Tanaka and Davis, 1988].

Earth-Based Radar Altimetry

Earth-based radar altimetry data are obtained on the principle that the absolute time delay of the leading edge of a radar echo gives the distance to the closest point on the planet's surface, usually located at or near the sub-Earth point [see Simpson et al., 1993]. Radar altimetry profiles have been derived from Goldstone observations during a number of Mars oppositions [Roth et al., 1980; Downs et al., 1982; Simpson et al., 1993]. The dimensions of each resolution cell vary with the parameters of the observations, however, resolution cells are on average ~10 km wide (0.16° in longitude) and ~120 km high (2.0° in latitude), an area of ~1200 km^2, for oppositions between 1973 and 1982 [see Downs et al., 1982]. The vertical uncertainty in the radar altimetry also varies. For the 1978 and 1980 oppositions the vertical uncertainty ranges from 50 to 280 m (for individual points in Chryse and Amazonis Planitia) with an average of ~160 m [see Downs et al., 1982, Table 1]. This is not sufficient to resolve small-scale, short-wavelength topographic features such as wrinkle ridges (often less than 10 km wide). The radar altimetry does, however, resolve large-scale, long-wavelength topographic variations such as regional slope, upon which wrinkle ridges are superposed.

Results

Wrinkle ridges are common landforms on the terrestrial planets. They are broad, low relief, morphologically complex features that may be composed of a number of superimposed landforms. Wrinkle ridges often consist of a composite of a broad arch and a narrow, asymmetric ridge, or these elements may occur independently of one another. They are sinuous, often occurring in segments of variable length, and are frequently regularly spaced. Their complex nature is reflected in the variety of kinematic models that have been proposed for their origin. It is generally agreed that wrinkle ridges are the result of compressional tectonism, resulting from folding and/or reverse or thrust faulting [Bryan, 1973; Howard and Muehlberger, 1973; Muehlberger, 1974; Maxwell et al., 1975; Lucchitta, 1976, 1977; Maxwell and Phillips, 1978; Sharpton and Head, 1982, 1988]. This interpretation is supported by studies of terrestrial analogs [Plescia and Golombek, 1986; Watters, 1988]; however, the relative role of folding and thrust faulting is unresolved [Golombek et al., 1991; Tanaka et al., 1991; Watters, 1991, 1993]. Although the average horizontal shortening across individual wrinkle ridges has been estimated using different model-dependent assumptions about the relative importance of folding and thrust faulting, all estimates are below 1 km [Watters, 1988; Golombek et al., 1991].

Apparent elevation offsets in photoclinometrically derived profiles across wrinkle ridges on Mars have been interpreted to be the result of deeply rooted thrust faults [Golombek et al., 1991; Plescia, 1991, 1993]. Golombek et al. [1991] suggest that the ridges accommodate vertical offsets between adjacent structural blocks. In their kinematic model, thrust faulting is the dominant mechanism in the formation of wrinkle ridges, and it accounts for the greatest component of horizontal shortening. Because wrinkle ridges are broad, low-relief features with relatively shallow slopes, the error introduced in photoclinometrically derived elevations through uncertainties in HDN and SLV may make it difficult to determine if a significant elevation difference across a ridge actually exists. In order to evaluate the sensitivity of the photoclinometric parameters, wrinkle ridges in a variety of locations on Mars were examined. An optimum location is in north-

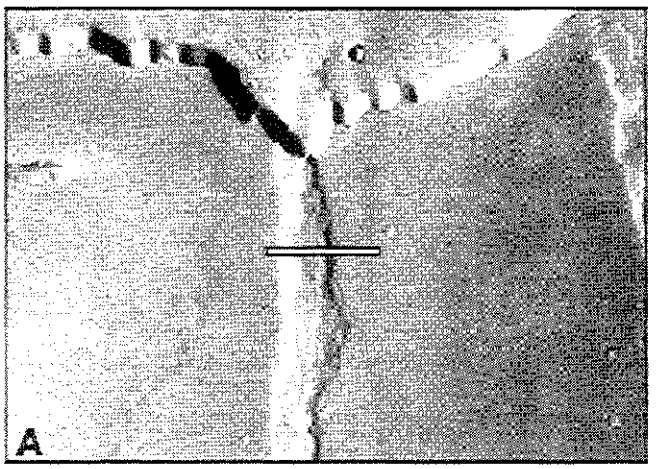

Figure 1a. Wrinkle ridge in northwest Lunae Planum (21°N, 71°W). Viking Orbiter image 519A06 (image resolution 194 m/pixel). The line indicates the location of the profiles shown in Figure 1b. The image is about 64 km wide.

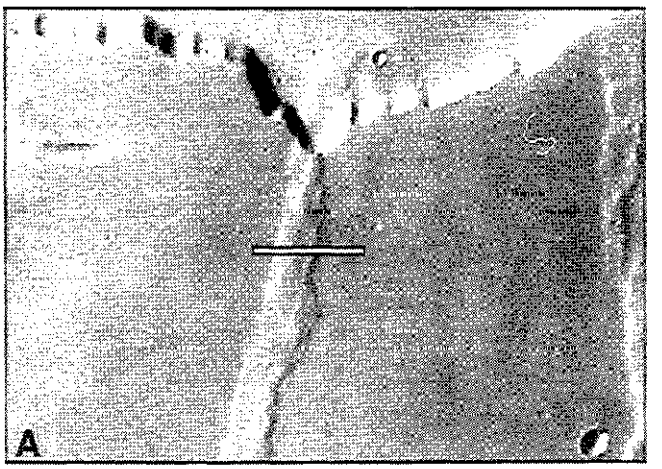

Figure 2a. Wrinkle ridge in northwest Lunae Planum (same location as Figure 1). Viking Orbiter image 555A04 (image resolution 191 m/pixel). The line indicates the location of the profiles shown in Figure 2b. Profiles were obtained at the same location shown in Figure 1a. The image is about 61 km wide.

west Lunae Planum where both medium and high resolution Viking Orbiter images are available. One ridge in northwest Lunae Planum was examined using three different images, two medium-resolution (519A06, 194 m/pixel, incidence angle 72°, red filter; 555A04, 191 m/pixel, incidence angle 73°, red filter) and one high-resolution (664A16, 42 m/pixel, incidence angle 78°, clear filter). The structure is a typical wrinkle ridge assemblage [see Watters, 1988] consisting of a first- and second-order ridge superimposed on a broad arch (Figures 1, 2, 3). Profile lengths are chosen, on the basis of photogeologic interpretation, to be the minimum necessary to span the full width of the ridge assemblage. This is to reduce uncertainties introduced by albedo variations and image calibration errors that scale with profile length. The SLV was determined by examining pixels in prominent shadows cast by scarps near the terminus of ridges. The HDN was estimated by determining the average of a 9x9 array of pixels located near the profile endpoints where the surface was judged, based on photogeology, to be horizontal. A 9x9 box (81 pixels) was used in order to increase the signal-to-noise ratio (averaging reduces the effects of random and digitization noise, and round off errors in calibration files). The elevation profiles we derived from the three images, all from the same location across the ridge, are extremely sensitive to small variations in the HDN (Figures 1, 2, 3). The sense of slope across a profile is completely reversed over a range in HDN as small as ±2 (HDN = 374) (Figure 3b). Comparable results were found for wrinkle ridges elsewhere in Lunae Planum, Arcadia Planitia, Coprates, and Hesperia Planum (see Appendix A). In contrast, elevation profiles are less sensitive to comparable variations in the SLV. Over a range in SLV of ±4 DN, the maximum change in elevation is 10 m (Figure 4). These results are not surprising because the SLV parameter is additive in the photometric equations, whereas the HDN parameter is multiplicative. The error in elevation introduced by the uncertainty in SLV was also checked by Tanaka and Davis [1988] in their study of simple graben in Syria Planum. They found photoclinometrically derived elevations to be within 10-15% of elevations determined by shadow measurements.

The large changes in the shape of photoclinometric profiles across wrinkle ridges that occur with small changes in HDN

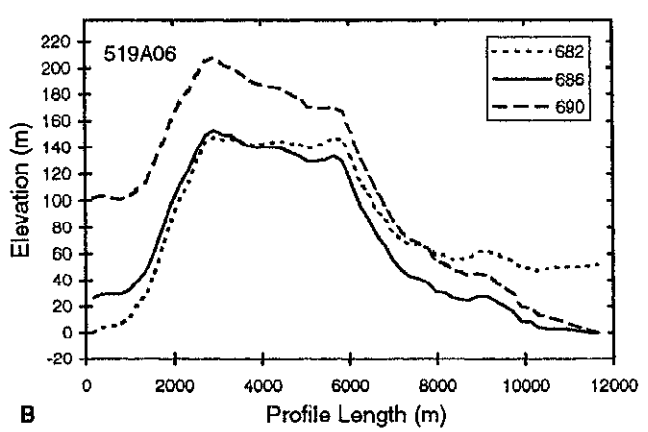

Figure 1b. Elevation profiles derived through photoclinometry. Profiles were generated for three different values of the HDN (shown in legend), holding all other parameters constant. The SLV is 455. Note that a change in HDN of 4 (0.6% change in HDN) reverses the sense of offset from one side of the profile to the other. Vertical exaggeration is 30:1.

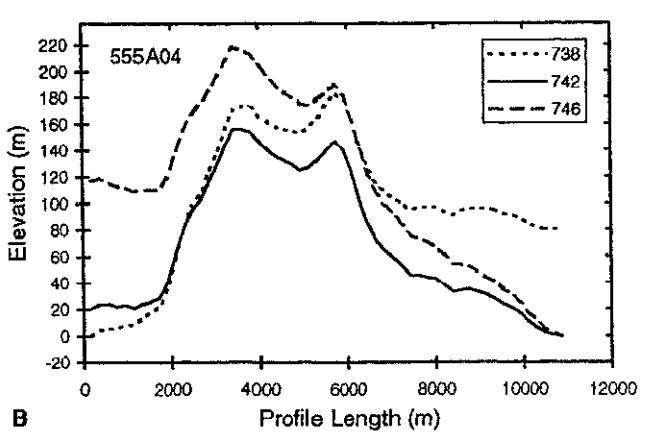

Figure 2b. Photoclinometric profiles were generated for three different values of the HDN (shown in legend), holding all other parameters constant. The SLV is 566. Note that a change in HDN of 4 (0.5% change in HDN) reverses the sense of offset from one side of the profile to the other. Vertical exaggeration is 30:1.

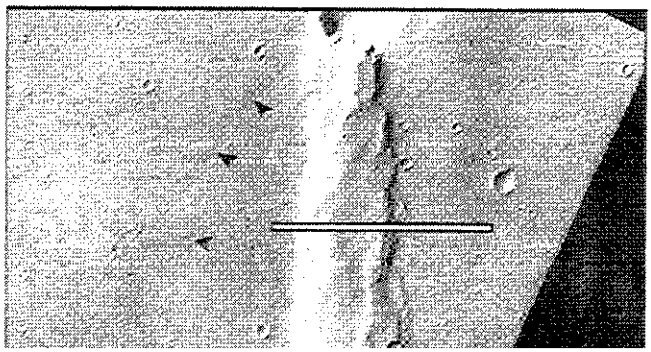

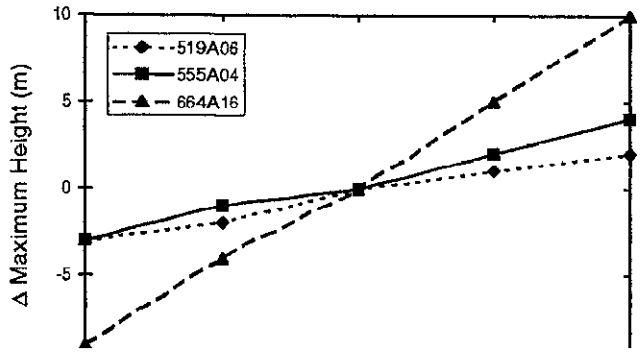
10
5
0
-5
Δ Maximum Height (m)
519A06
555A04
664A16

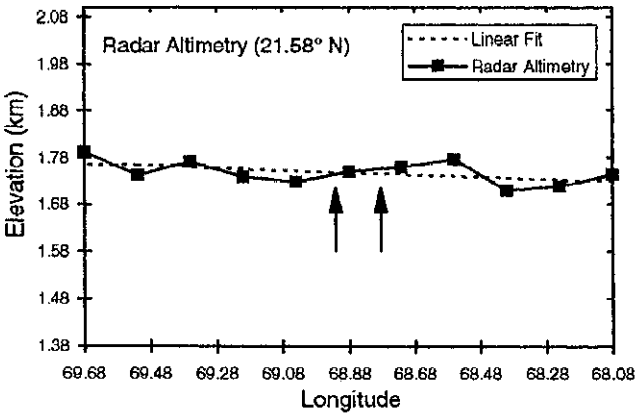

Figure 6. Radar altimetry data crossing a wrinkle ridge in northern Lunae Planum (21.58°N, 68.85°W). The regional slope is defined by a linear least squares fit to the radar altimetry (m=0.024; b=0.123). Arrows indicate the location of profiles shown in Figures 7 and 8. Altimetry is relative to the 6 mbar surface, and the vertical exaggeration is 30:1.

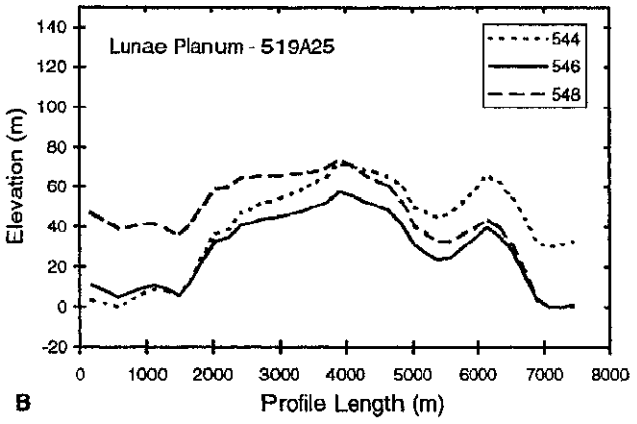

Figure 7b. Photoclinometric profiles derived using three different values of the HDN (shown in legend), holding all other parameters constant (SLV=423). Vertical exaggeration is 30:1.

Controlled photoclinometric profiles were also generated across wrinkle ridges in Arcadia Planitia and Coprates (Appendix B). Comparing the controlled profiles (Figures B4 and B8) with the uncontrolled profiles (Figures B3 and B7), it is shown that an error in HDN of as little as ±1 can produce a significant error in photoclinometrically derived elevations that result in apparent elevation offsets and inaccurate dimensional data, particularly maximum relief of a ridge.

Implications

Kinematic Models

The kinematic model for the origin of planetary wrinkle ridges proposed by Golombek et al. [1991], based on apparent elevation offsets in the topographic profiles generated across wrinkle ridges on Mars and the Moon, involves motion on deeply rooted thrust faults that separates crustal material into structural blocks at different elevations. This model was used as the basis for estimating horizontal shortening across wrinkle ridges. Golombek et al. [1991] concluded that shortening due to faulting dominates over shortening due to folding and thus folding is secondary to faulting in the formation of wrinkle ridges. The model has been adopted in subsequent studies of martian wrinkle ridges by Plescia [1991, 1993].

Because of the uncertainty in the HDN, the existence of elevation offsets across wrinkle ridges studied here cannot be determined with any confidence using photoclinometry alone. Although the Earth-based radar altimetry cannot resolve individual wrinkle ridges, if thrust faults beneath the ridges have separated the ridged plains into a series of broad, gently sloping structural blocks with different elevations, evidence of this should be apparent in the radar altimetry. We exam-

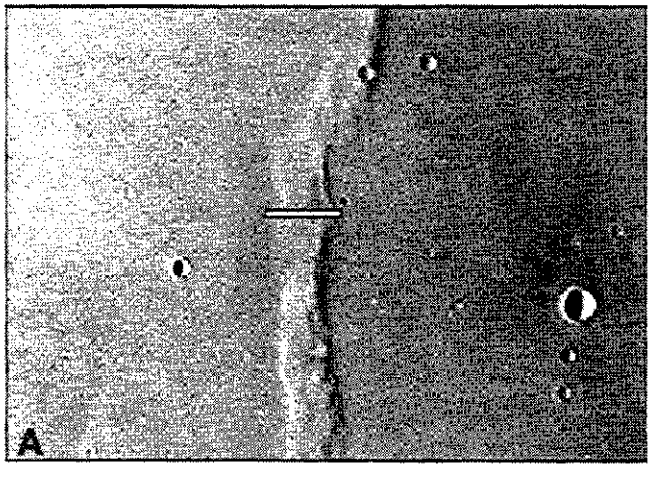

Figure 7a. Wrinkle ridge in northern Lunae Planum (21.58°N, 68.85°W). Viking Orbiter image 519A25 (image resolution 186 m/pixel). The line indicates the location of the profiles shown in Figure 7b and corresponds with the track of radar altimetry data shown in Figure 6. The image is about 59 km wide.

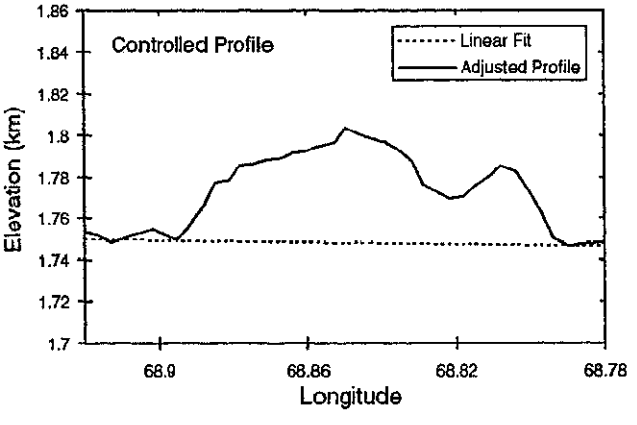

Figure 8. Controlled photoclinometric profile across a wrinkle ridge in northern Lunae Planum (21.58°N, 68.85°W). The HDN was adjusted until the elevation difference in the photoclinometric profile between one side of the ridge and the other matched the elevation difference in corresponding points in the linear fit to the radar altimetry (see Figure 6) (HDN=546.2). Next, this adjusted profile was tied to the 6 mbar frame of reference by adding it to the corresponding points in the linear fit to the radar altimetry. The dotted line is the linear fit to the radar altimetry (see Figure 6). Elevation is relative to the 6 mbar surface, and the vertical exaggeration is 30:1. Profile was obtained in the same location as in Figure 7a.

ined radar profiles across ridged plains in northern Lunae Planum, northern Amazonis and Arcadia Planitia, and Coprates (see Figures 5, B1, and B5). We find no topographic evidence, at the resolution of the radar altimetry (average vertical uncertainty of ~160 m), that wrinkle ridges accommodate vertical offsets between adjacent structural blocks of ridged plains material as suggested by Golombek et al. [1991] and Plescia [1991, 1993]. The results presented here suggest that when elevation offsets occur from one side of a ridge to the other, they are likely due to regional slope rather than the localized surface manifestation of a thrust fault. Elevation offsets, however, may also result from other processes, such as the ponding of lava flows. There is evidence in lunar mare basins and on the ridged plains of Mars of flows in proximity to or ponded by wrinkle ridges [Bryan, 1973; Watters, 1991]. On Mars, the accumulation of windblown material against the flank of a ridge could also result in an elevation offset. The accumulation of volcanic or windblown material along a wrinkle ridge could obscure an elevation offset that is structural in origin. Although no clear surface expression of thrust faults have been found, thrust faulting likely plays an important role in the formation of wrinkle ridges. This assumption is based on comparisons with terrestrial analogs [Plescia and Golombek, 1986], particularly those in the continental flood basalts of the Columbia Plateau [Watters, 1988].

The anticlinal ridges of the Columbia Plateau occur in a sequence of basalt flows emplaced on a thick accumulation of poorly consolidated sediments [see Reidel et al., 1989a, b; Campbell, 1989; Watters, 1989, 1991; Schultz and Watters, 1995]. These anticlines are similar in scale and morphology to planetary wrinkle ridges [see Watters, 1988], and like wrinkle ridges on Mars and Venus, they are regularly spaced [Watters, 1992]. Because wrinkle ridges on the Moon are known to occur in mare basalts, and those on Mars, Venus, and Mercury are thought to occur in basalt-like sequences, the Columbia anticlines are probably the best terrestrial analogs to planetary wrinkle ridges [Watters, 1988, 1992]. The kinematic model for the origin of wrinkle ridges adopted here is one that is consistent with models for the origin of the Columbia anticlines and the morphology of the martian ridges investigated in this study. A horizontal compressive load coupled with a layer instability between the basalt (or basalt-like) sequence and the underlying sediments or megaregolith results in buckling. Concentric folds develop with a large component of simple shear strain. As fold amplification increases, the concentric folds close, which leads to the development of thrust faulting [see Watters, 1988, Figure 13].

Estimates of Horizontal Shortening

Golombek et al. [1991] and Plescia [1991, 1993] estimated the horizontal shortening across martian wrinkle ridges due to thrust faulting and folding. Their estimates of shortening due to thrust faulting are based solely on elevation offsets observed in photoclinometric profiles. However, as described above, the elevation offsets may result from ambiguity in the HDN. Because there is no unambiguous surface expression of thrust faulting associated with martian or other planetary wrinkle ridges, estimating the contribution of thrust faulting to the total crustal shortening across these structures is difficult. Estimates of horizontal shortening, however, can be made if it is assumed that all shortening is reflected in the topographic expression of the wrinkle ridge. In this case, the horizontal shortening (Δl) is given by

$$\Delta l = l_d - l_u \tag{2}$$

where l_d is the deformed line length and l_u is the undeformed line length, and unit shortening or compressive strain (ε) is given by

$$\varepsilon = \Delta l / l_u \tag{3}$$

The error in estimating shortening by restoring deformed topography to a planar surface, where a thrust fault is involved, is dependent on the angle of the fault [see Dahlstrom, 1969]. If a low-angle thrust fault is involved, the error in the estimated shortening may be large. Thus estimates of horizontal shortening across wrinkle ridges obtained using this method may be only lower limits of the total shortening.

The undeformed line length (l_u) was determined by summing the distance between points along the surface of the wrinkle ridge in the photoclinometric profile. The deformed line length (l_d) is the straight-line distance between the endpoints of the profile that define the limits of the ridge. The errors associated with estimating Δl are large because the confidence in the length measurement is assumed to be on the order of one-half the pixel dimension at each end of the profile (total error is thus 1 pixel). This is reasonable, since the edges of a ridge are expected to fall somewhere within the two pixels that define the profile endpoints. Both the controlled and uncontrolled profiles were used to estimate the shortening. In the case of the uncontrolled profiles, the horizontal shortening was estimated using profiles with the least apparent elevation offset. However, since offsets are ignored in these estimates, using uncontrolled profiles with apparent elevation offsets has no significant effect on the measurement. Estimates of the horizontal shortening for the wrinkle ridges investigated in this study range from 1 to 71 m with an average of 12 m (n=16) (Table 1). This is consistent with the range of shortening (due to folding alone) obtained by Golombek et al. [1991] and Plescia [1993] for the wrinkle ridges they studied. It is important to note, however, that the estimates of shortening made in this study are all far below the error in the measurement (Table 1). Inspecting the estimated errors associated with Δl (Table 1) suggests that the horizontal shortening must exceed the image resolution by at least a factor of 2 to be reliably measured using this method.

The horizontal shortening across the ridges studied in Arcadia Planitia is consistently lower than estimates for ridges in Lunae Planum, Coprates, and Hesperia Planum (see Table 1). The topography of these ridges is subdued relative to those investigated elsewhere (Figures A1-A3, B3, and B4), as reflected in the width to maximum height ratio (w/h) of the Arcadia ridges, which is about 130 compared to about 70 for ridges in Lunae Planum, 50 for ridges in Coprates, and 60 for ridges in Hesperia Planum. The average spacing of the Arcadia ridges, however, is consistent with ridge spacing in Lunae Planum, Coprates, and other ridged plains units throughout Tharsis [see Watters, 1991]. The subdued nature of the Arcadia ridges may be a result of post ridge formation lava flow emplacement and erosion from flooding. Lava flows of the Elysium Formation have partly covered Hesperian age ridged plains material [Scott and Tanaka, 1986; Greeley and Guest, 1987; Plescia, 1993] and embay wrinkle ridges and fill intra-ridge areas [see Plescia, 1993]. Therefore some of the

Table 1. Wrinkle Ridge Dimensions and Estimates of Shortening

Viking Image	Resolution, m/pixel	Latitude	Longitude	Maximum Relief, m	l_d, m	l_u, m	w/h	Δl, m
				Arcadia Planitia				
545A49	145	20.68° N	179.4° W	61	12434±145	12436±145	204	2±290*
545A25	153	26.15° N	176.75° W	46	4765±154	4767±154	104	2±308
545A25	153	26.10° N	177.65° W	32	2609±153	2610±153	82	1±306
545A25	153	27.17° N	177.23° W	33	4600±153	4601±153	139	1±306
				Coprates				
608A49	217	18.99° S	72.0° W	196	7626±218	7637±220	39	11±438*
608A49	217	21.59° S	71.97° W	261	6289±217	6315±221	24	26±438
608A45	212	24.11° S	80.12° W	182	6788±212	6799±214	37	11±426
608A24	202	26.53° S	80.0° W	174	15589±202	15596±203	90	7±405
				Hesperia Planum				
365S64	220	28.4° S	239.6° W	94	5943±220	5948±221	63	5±441
356S64	220	29.47° S	241.3° W	351	11843±219	11914±230	34	71±449
365S62	220	30.81° S	239.37° W	56	4395±220	4398±221	79	3±441
365S62	220	31.19° S	239.13° W	83	6592±220	6595±221	79	3±441
				Lunae Planum				
519A25	186	21.58° N	68.85° W	60	5774±186	5777±187	96	3±373*
519A26	188	19.93° N	64.73° W	103	10523±188	10530±189	102	7±377
520A25	186	22.02° N	61.68° W	288	7629±186	7659±191	27	30±377
519A06	194	21.04° N	71.0° W	153	9529±194	9537±195	62	8±389
555A04	191	21.04° N	71.0° W	156	9529±191	9539±193	61	10±384
664A16	42	21.04° N	71.0° W	159	9531±42	9548±45	60	17±87

*Based on photoclinometric profile controlled with Earth-based radar. Here w/h is the ridge width to maximum height ratio. Error estimates on l_d are based on a confidence of ½ the pixel dimension at each end of the profile (total error one pixel), and those on l_u additionally include ±7.5% of the photoclinometrically derived elevations [see Tanaka and Davis, 1988]. Error estimates on Δl are the combined errors from l_d and l_u.

structural relief of the wrinkle ridges may be obscured by the embaying lava flows. There is also evidence of flooding of the ridged plains of Amazonis and Arcadia Planitia. Amazonian age outflow channels dissect ridged plains material, leaving in some cases only what appear to be remnants of wrinkle ridges [see Scott and Tanaka, 1986]. Thus many of the Arcadia and Amazonis ridges may be partially buried by lava flows, while others have suffered some degree of erosion. This must be carefully considered in making any estimates of local or regional crustal shortening since only a portion of the original structural relief of the ridges is preserved.

Discussion

It has been suggested that thrust faults associated with wrinkle ridges may penetrate most of the martian lithosphere [Zuber and Aist, 1990; Golombek et al., 1991; Tanaka et al., 1991]. Tanaka et al. [1991] conclude that if the deformed materials are dry, low-cohesion rocks, thrust faults associated with wrinkle ridges might extend to a depth of 10 km if they accommodate compressional strain on the order of 10^{-2}. If strong, cohesive volcanic flows underlain by weaker material (i.e., a megaregolith) are involved, they argue that faulting beneath wrinkle ridges could penetrate more of the lithosphere, since faulting would propagate downward in the megaregolith until stress levels in the volcanic flows were sufficient to produce failure. In this model, Tanaka et al. [1991] suggest that deep-seated faulting would lead to fewer ridges accommodating greater shortening. They argue that this can explain observations of Plescia [1991] that more widely spaced "large ridges" with greater shortening occur in thicker units on western Lunae Planum and "smaller ridges" with less shortening occur in thinner plains units on eastern Lunae Planum.

Results presented here indicate that there is no evidence that ridges in western Lunae Planum (Figures 1, 2, 3) exhibit greater vertical relief and accommodate greater amounts of shortening than the ridges in eastern Lunae Planum. In fact, a ridge in eastern Lunae Planum (Figure A12) has the greatest relief and largest estimated shortening of the ridges studied in Lunae Planum (Table 1). Although the average ridge spacing in eastern Lunae Planum (mode 20 km) is less than the average spacing throughout much of the rest of Lunae Planum (mode 35 km) [see Watters, 1991, Table 1], there is no evidence that larger ridges are more widely spaced than smaller ones. A relationship between ridge spacing and the thickness of the ridged plains material on Lunae Planum and elsewhere on Mars, however, can be argued [see Watters, 1993]. This relationship supports models for the origin of wrinkle ridges that involve buckling at a critical wavelength of folding where ridge spacing is directly related to the thickness of the ridged plains material [Watters, 1991; Watters and Schultz, 1995].

The absence of a clear surface expression of the thrust faulting that is likely to be associated with wrinkle ridge formation (i.e., elevation offsets) does not support models involving deeply rooted faults. This is supported by recent

geophysical studies of the subsurface structure of the Columbia Plateau. Analysis of newly acquired seismic and gravity data by Saltus [1993] and Jarchow et al. [1994] shows no evidence of deeply rooted thrust faults beneath the anticlinal ridges. The thrust faults associated with the anticlines are confined to the deformed Columbia River Basalts. Applying this analog to wrinkle ridges on Mars and on the other terrestrial planets, the thrust faults that are likely to be involved in their formation may not be rooted in the lithosphere or the dominant mode of deformation [Watters, 1988, 1991, 1993]. In addition, many wrinkle ridges on Mars have been affected by shallow-depth mechanical discontinuities introduced by buried craters. Buried craters strongly influence and often localize the formation of some wrinkle ridges. This is clearly reflected by circular trending ridges that are common in ridged plains units, particularly those in Hesperia Planum (see Figure A8) [also see Watters, 1993, Figure 6]. The influence that shallow-depth mechanical discontinuities can have on wrinkle ridge formation does not support thick-skinned deformation models involving thrust faults that penetrate the lithosphere [Zuber and Aist, 1990; Golombek et al., 1991; Tanaka et al., 1991].

If wrinkle ridges are formed by folding and thrust faulting confined to surface layers, as appears to be the case for the anticlinal ridges of the Columbia, then compression in the lithosphere must be accommodated by a different deformational mechanism. Strike-slip faults are known to be associated with the Columbia anticlines [Anderson, 1987; Watters, 1992]. Indirect evidence also suggests that strike-slip faulting is associated with the formation of wrinkle ridges on Mars [Schultz, 1989; Watters, 1992]. The geometric relationship between ridges and strike-slip faults on the Columbia Plateau and Mars is consistent with the Coulomb-Anderson model [Anderson, 1951] where folding and thrust faulting is predicted perpendicular to the maximum principal stress, and strike-slip faulting is predicted along conjugate planes bisected by the maximum and the minimum principal stresses [Watters, 1992]. Compression in the shallow crustal layers possibly is accommodated in the lithosphere primarily by strike-slip faulting. Since the Coulomb-Anderson model requires that the direction of least compression change from vertical to horizontal for strike-slip faulting to develop, an inhomogeneous stress field is necessary. Such a stress field could result from a more rapid increase of the vertical stress relative to the horizontal stresses with depth [see Crosson, 1972]. If this is the case, folding and thrust faulting would be expected at shallow depths where the least compressive stress is vertical, and strike-slip faulting would be expected at greater depths where the intermediate stress is vertical.

Conclusions

Photoclinometric profiles across wrinkle ridges are very sensitive to small variations in the HDN. The sense of slope can be completely reversed over a relatively narrow range in HDN (as low as ±1 DN). The photoclinometrically derived elevations are much less sensitive to comparably small variations in the SLV. These results are true for wrinkle ridges examined in Lunae Planum, Arcadia Planitia, Coprates, and Hesperia Planum. The sensitivity of the photoclinometric profiles across wrinkle ridges to the HDN is a direct result of the shallow slopes on these relatively broad, low-relief features. Because of the uncertainty in the HDN, for the features examined here the existence of an elevation offset from one side of a wrinkle ridge to the other cannot be confidently determined through photoclinometry alone. Earth-based radar altimetry profiles were examined to evaluate the long- wavelength topography associated with wrinkle ridges. These profiles reveal no evidence of elevation offsets at the resolution of radar altimetry.

The results of this study show that the available topographic data do not support kinematic models for the origin of planetary wrinkle ridges that involve deeply rooted thrust faults that separate crustal material into structural blocks at different elevations [Golombek et al., 1991; Plescia, 1991, 1993; Tanaka et al., 1991]. However, a kinematic model consistent with models for the origin of the anticlinal ridges of the Columbia Plateau, probably the best terrestrial analogs to martian wrinkle ridges, is consistent with these data. This model involves buckling of shallow crustal layers into concentric folds that close, which leads to the development of thrust faulting. Estimates of the horizontal shortening across the wrinkle ridges studied, determined by restoring deformed topography to a planar surface, are all far below the errors in the measurements (Table 1). This is due predominantly to the uncertainty in the measurement of the profiles lengths. For confident estimates to be obtained, the horizontal shortening must exceed the image resolution by at least a factor of 2. Thus the results presented here demonstrate that horizontal shortening less than 100 to 200 m across wrinkle ridges on Mars cannot be accurately determined using the available data. The availability of higher resolution images and laser altimetry data from Mars Global Surveyor will make more reliable estimates possible. Because the extent and nature of the thrust faults involved in ridge formation are uncertain, estimates of shortening obtained in this study are only lower limits. On the basis of the influence of shallow subsurface structures, particularly buried craters, on the localization of many wrinkle ridges on Mars, it is likely that the thrust faults associated with wrinkle ridges are confined to the ridged plains material and do not extend into the lithosphere. This is supported by recent geophysical studies of the Columbia anticlines, which show no evidence of thrust faulting below the Columbia River Basalts. Strike-slip faults associated with the formation of wrinkle ridges, and the anticlinal ridges of the Columbia, may initiate in the lithosphere where they accommodate the horizontal shortening reflected in the crust.

Appendix A

Wrinkle ridges in Arcadia Planitia, Coprates, Hesperia Planum, and Lunae Planum were studied. Figures A1-A12 illustrate that photoclinometric profiles across wrinkle ridges, occurring in all the major units of ridged plains material on Mars, are sensitive to minor changes in the HDN value. Note that small variations in HDN completely reverse the sense of apparent offset from one side of the profiles to the other. This reflects the fact that wrinkle ridges on Mars, although morphologically complex, are all generally broad, low-relief structures with shallow slopes. With such shallow slopes, the limits of the sensitivity of the method are approached [Davis and Soderblom, 1984; Tanaka and Davis, 1988].

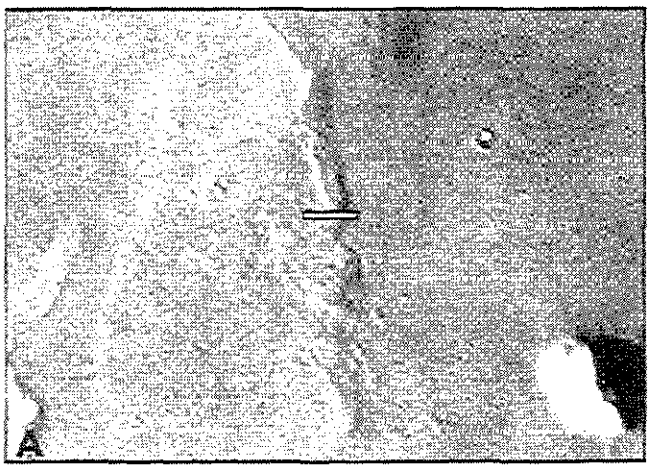

Figure A1a. Wrinkle ridge in Arcadia Planitia (26.1°N, 177.65°W). Viking Orbiter image 545A25 (image resolution 153 m/pixel). The line indicates the location of the profiles shown in Figure A1b. The image is about 32 km wide.

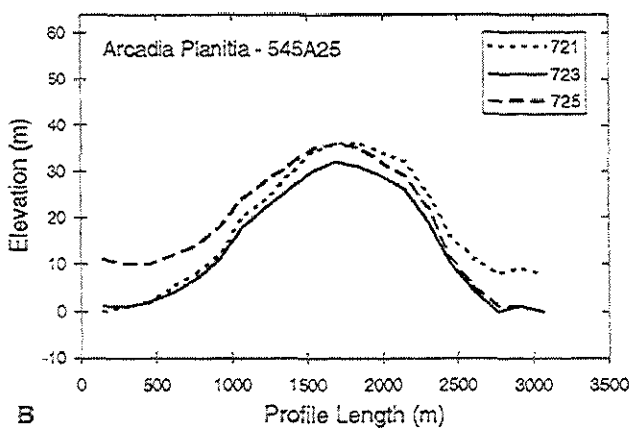

Figure A1b. Photoclinometric profiles derived using three different values of the HDN (shown in legend), holding all other parameters constant (SLV=442). Vertical exaggeration is 30:1.

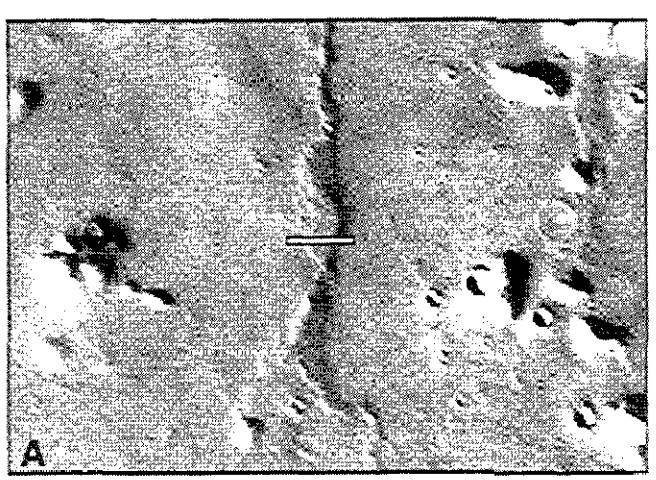

Figure A2a. Wrinkle ridge in Arcadia Planitia (26.15°N, 176.75°W). Viking Orbiter image 545A25 (image resolution 153 m/pixel). The line indicates the location of the profiles shown in Figure A2b. The image is about 45 km wide.

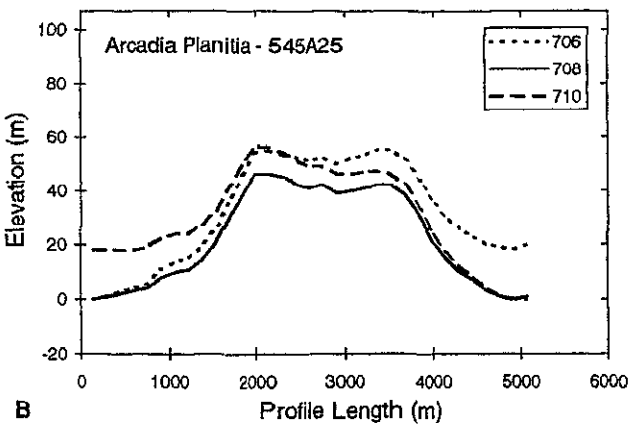

Figure A2b. Photoclinometric profiles derived using three different values of the HDN (shown in legend), holding all other parameters constant (SLV=442). Vertical exaggeration is 30:1.

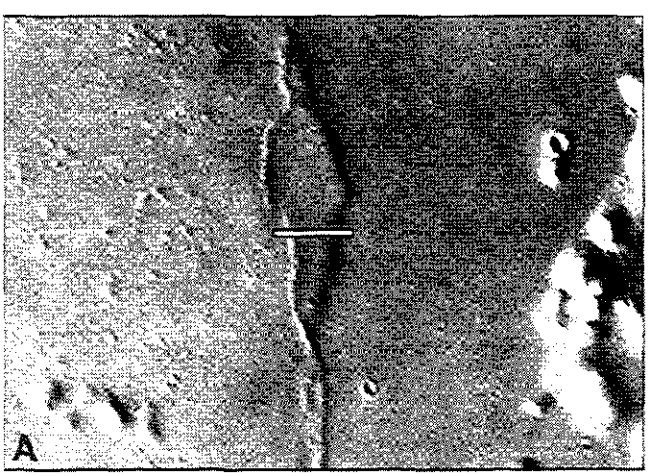

Figure A3a. Wrinkle ridge in Arcadia Planitia (27.17°N, 177.23°W). Viking Orbiter image 545A25 (image resolution 153 m/pixel). The line indicates the location of the profiles shown in Figure A3b. The image is about 43 km wide.

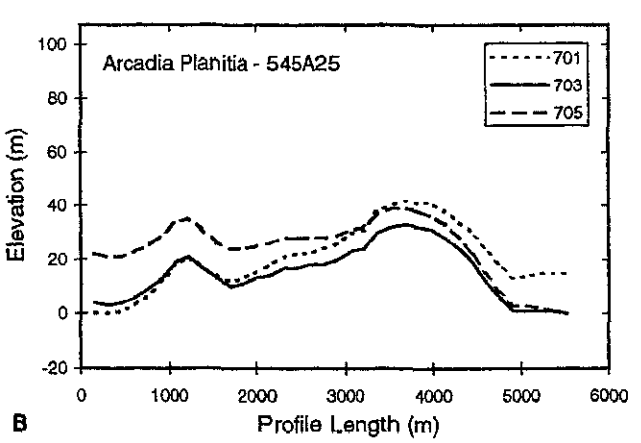

Figure A3b. Photoclinometric profiles derived using three different values of the HDN (shown in legend), holding all other parameters constant (SLV=432). Vertical exaggeration is 30:1.

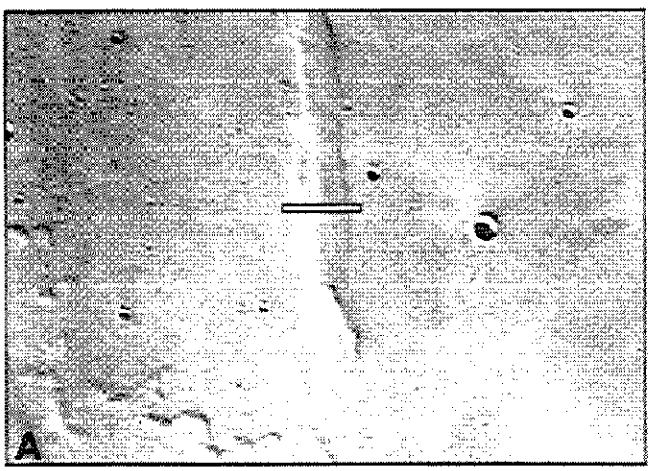

Figure A4a. Wrinkle ridge in Coprates (24.11°S, 80.12°W). Viking Orbiter image 608A45 (image resolution 212 m/pixel). The line indicates the location of the profiles shown in Figure A4b. The image is about 72 km wide.

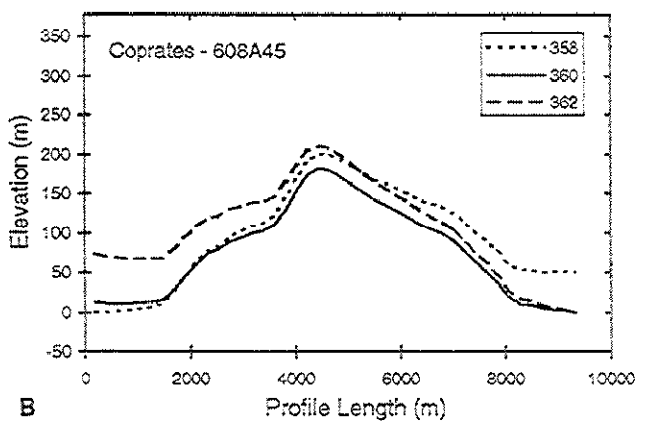

Figure A4b. Photoclinometric profiles derived using three different values of the HDN (shown in legend), holding all other parameters constant (SLV=217). Vertical exaggeration is 15:1.

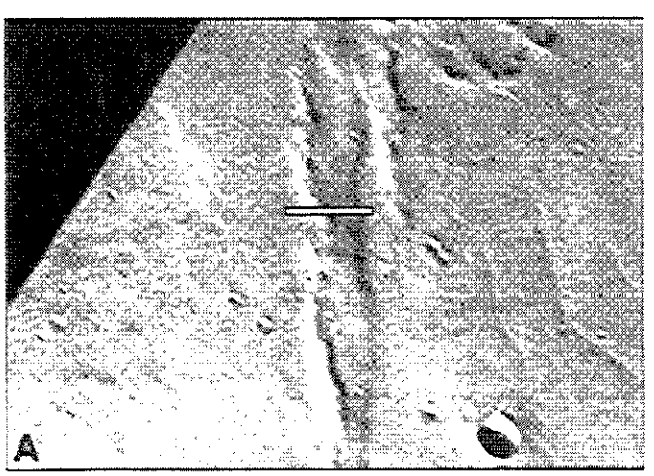

Figure A5a. Wrinkle ridge in Coprates (21.59°S, 71.97°W). Viking Orbiter image 608A49 (image resolution 217 m/pixel). The line indicates the location of the profiles shown in Figure A5b. The image is about 49 km wide.

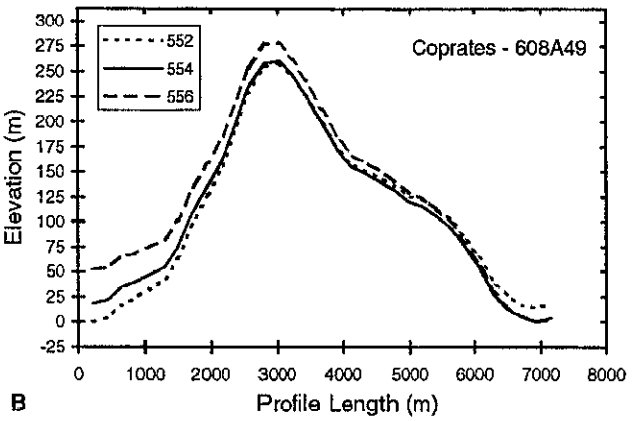

Figure A5b. Photoclinometric profiles derived using three different values of the HDN (shown in legend), holding all other parameters constant (SLV=274). Vertical exaggeration is 15:1.

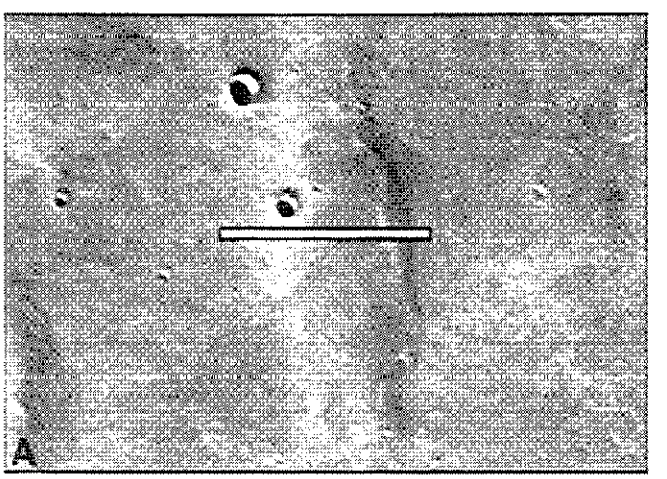

Figure A6a. Wrinkle ridge in Coprates (26.53°S, 80.0°W). Viking Orbiter image 608A24 (image resolution 202 m/pixel). The line indicates the location of the profiles shown in Figure A6b. The image is about 49 km wide.

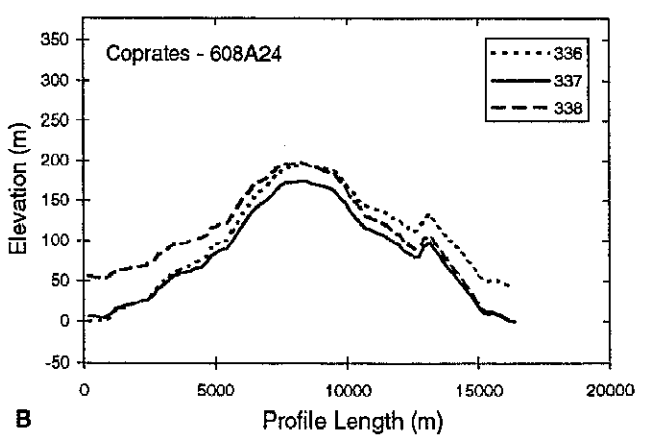

Figure A6b. Photoclinometric profiles derived using three different values of the HDN (shown in legend), holding all other parameters constant (SLV=205). Vertical exaggeration is 30:1.

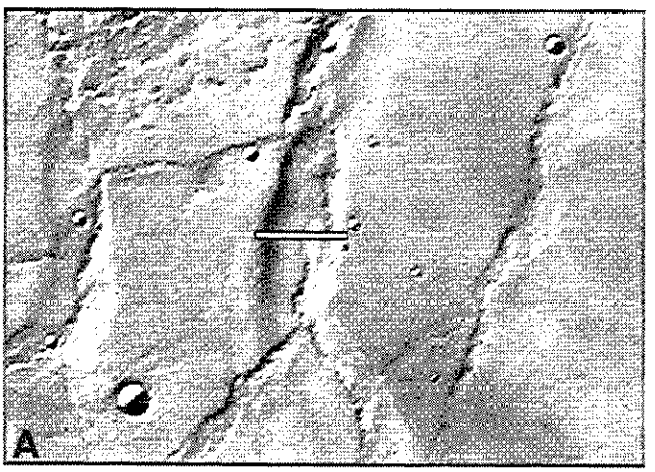

Figure A7a. Wrinkle ridge in Hesperia Planum (29.47°S, 241.3°W). Viking Orbiter image 365S64 (image resolution 220 m/pixel). The line indicates the location of the profiles shown in Figure A7b. The image is about 86 km wide.

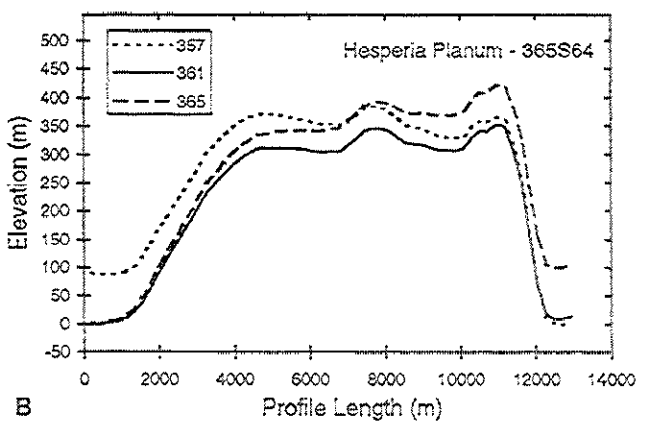

Figure A7b. Photoclinometric profiles derived using three different values of the HDN (shown in legend), holding all other parameters constant (SLV=97). Vertical exaggeration is 15:1.

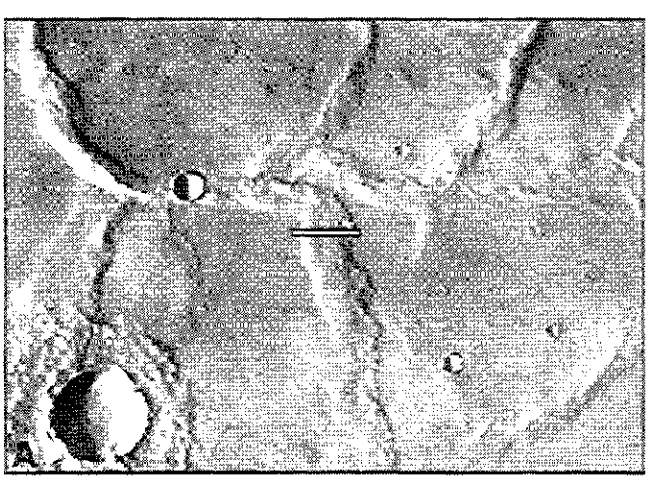

Figure A8a. Wrinkle ridge in Hesperia Planum (28.4°S, 239.6°W). Viking Orbiter image 365S64 (image resolution 220 m/pixel). The line indicates the location of the profiles shown in Figure A8b. The image is about 62 km wide.

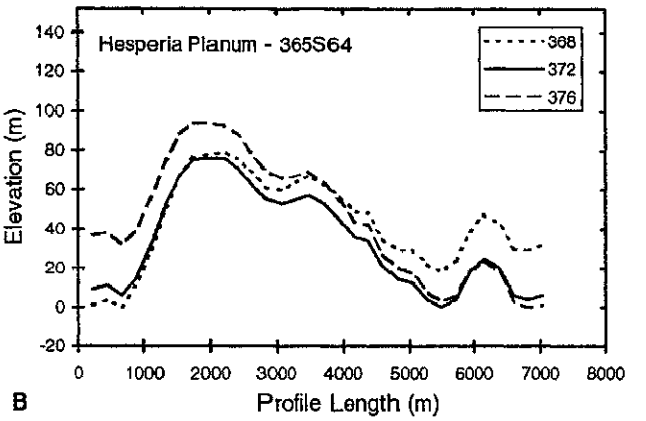

Figure A8b. Photoclinometric profiles derived using three different values of the HDN (shown in legend), holding all other parameters constant (SLV=116). Vertical exaggeration is 30:1.

Appendix B

Figures B1-B8 demonstrate the method employed here to constrain the HDN value by using Earth-based radar altimetry. In addition, radar data are used to tie the photoclinometric profiles to the Mars 6 mbar frame of reference.

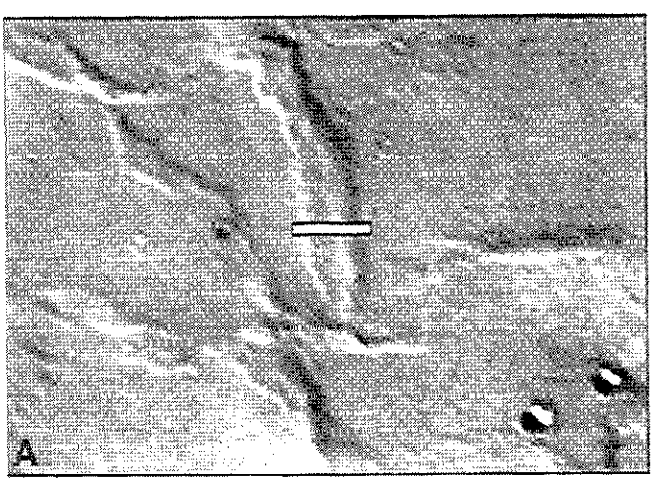

Figure A9a. Wrinkle ridge in Hesperia Planum (30.81°S, 239.37°W). Viking Orbiter image 365S62 (image resolution 220 m/pixel). The line indicates the location of the profiles shown in Figure A9b. The image is about 36 km wide.

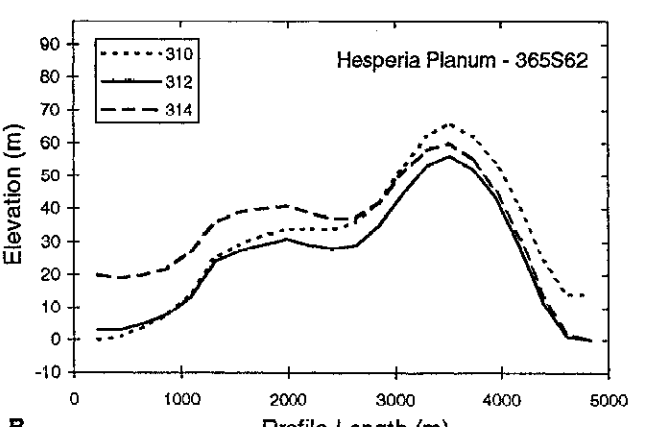

Figure A9b. Photoclinometric profiles derived using three different values of the HDN (shown in legend), holding all other parameters constant (SLV=104). Vertical exaggeration is 30:1.

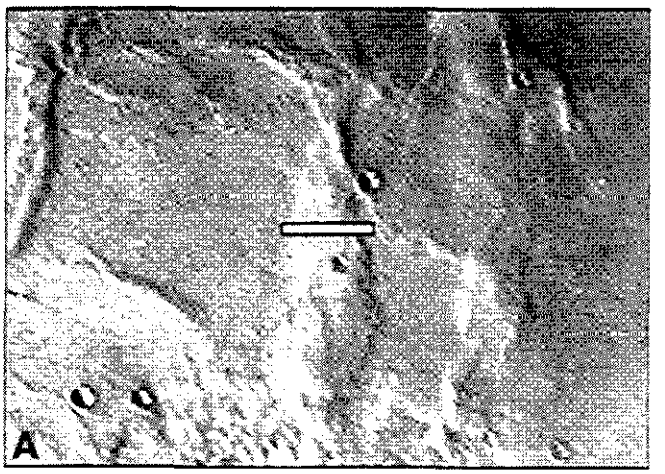

Figure A10a. Wrinkle ridge in Hesperia Planum (31.19°S, 239.13°W). Viking Orbiter image 365S62 (image resolution 220 m/pixel). The line indicates the location of the profiles shown in Figure A10b. The image is about 50 km wide.

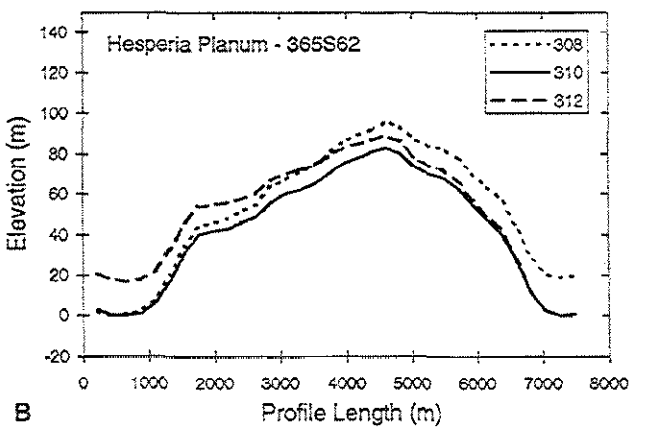

Figure A10b. Photoclinometric profiles derived using three different values of the HDN (shown in legend), holding all other parameters constant (SLV=104). Vertical exaggeration is 30:1.

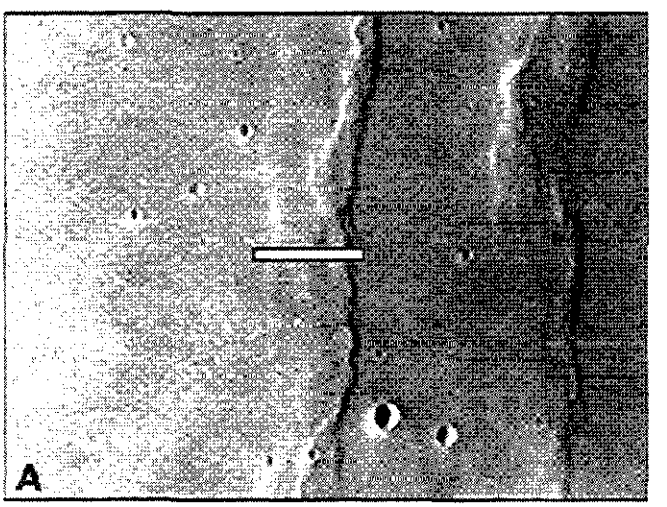

Figure A11a. Wrinkle ridge in Lunae Planum (19.93°N, 64.73°W). Viking Orbiter image 519A26 (image resolution 188 m/pixel). The line indicates the location of the profiles shown in Figure A11b. The image is about 65 km wide.

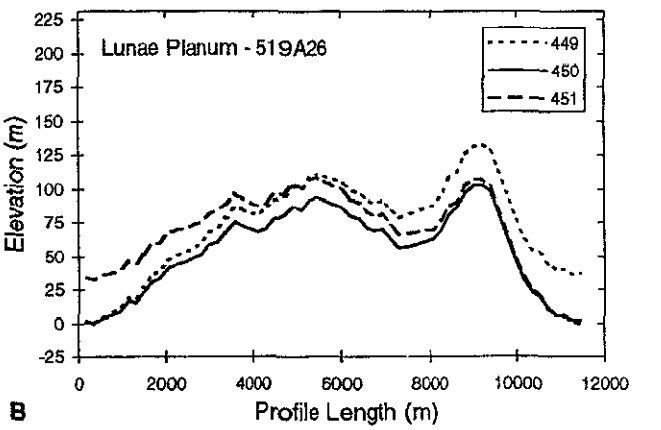

Figure A11b. Photoclinometric profiles derived using three different values of the HDN (shown in legend), holding all other parameters constant (SLV=372). Vertical exaggeration is 30:1.

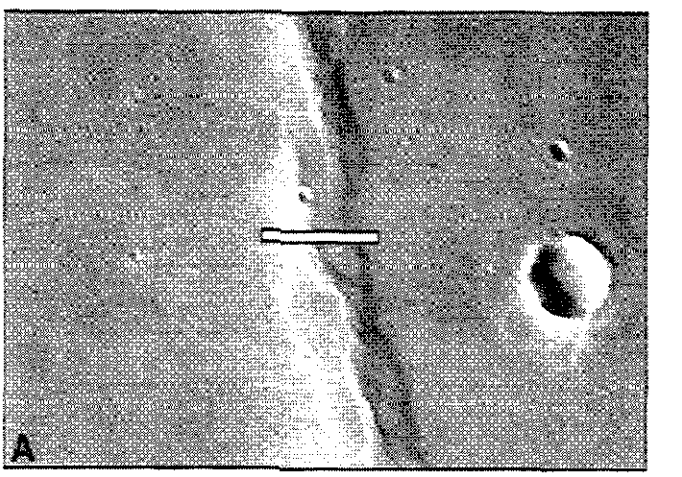

Figure A12a. Wrinkle ridge in Lunae Planum (22.02°N, 61.68°W). Viking Orbiter image 520A25 (image resolution 186 m/pixel). The line indicates the location of the profiles shown in Figure A12b. The image is about 44 km wide.

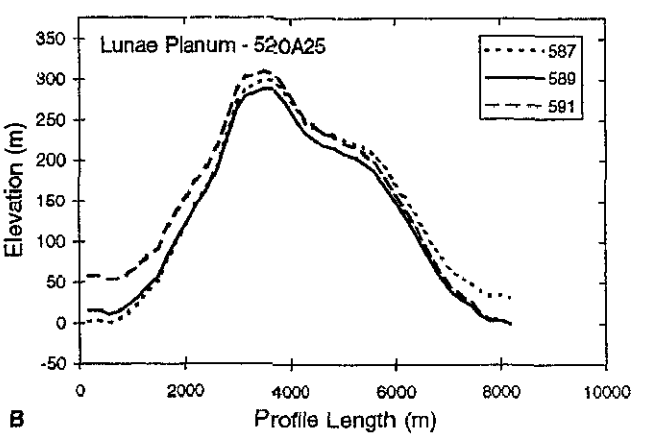

Figure A12b. Photoclinometric profiles derived using three different values of the HDN (shown in legend), holding all other parameters constant (SLV=434). Vertical exaggeration is 15:1.

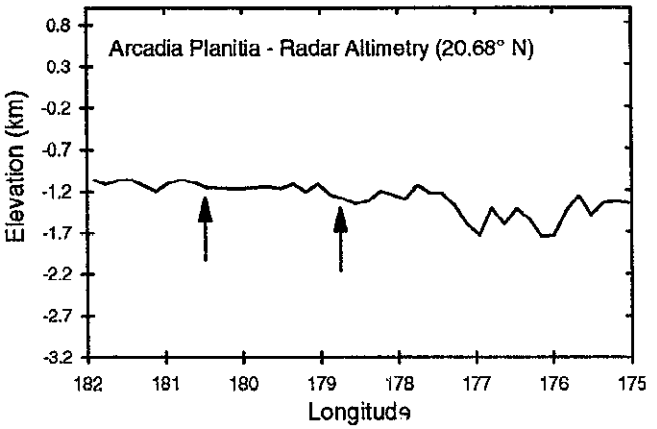

Figure B1. Earth-based radar altimetry profile across Arcadia Planitia. The profile is located at 20.68°N and was derived from Goldstone radar data acquired in 1982. An eastward dipping regional slope is reflected in the altimetry data. Arrows indicate the location of the profile shown in Figure B2. Altimetry is relative to the 6 mbar surface, and the vertical exaggeration is 60:1.

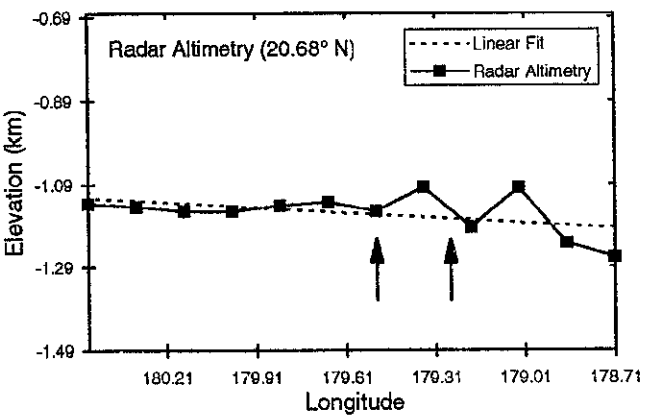

Figure B2. Goldstone radar altimetry data crossing a wrinkle ridge in Arcadia Planitia (20.68°N, 179.4°W). The regional slope is defined by a linear least squares fit to the radar altimetry (m=0.042; b=-8.648). Arrows indicate the location of profiles shown in Figures B3 and B4. Altimetry is relative to the 6 mbar surface, and the vertical exaggeration is 30:1.

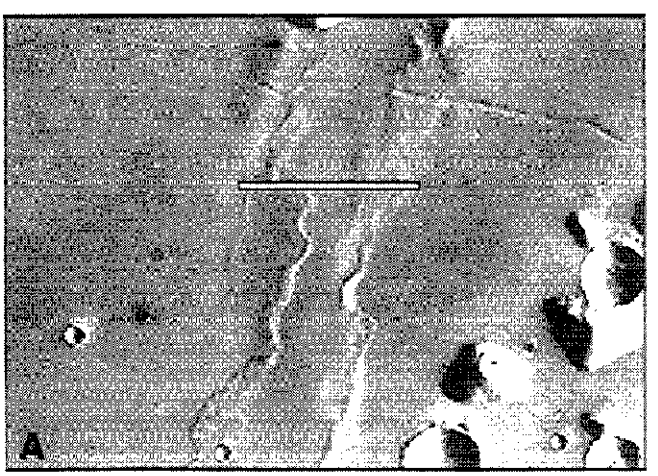

Figure B3a. Wrinkle ridge in Arcadia Planitia (20.68°N, 179.4°W). Viking Orbiter image 545A49 (image resolution 145 m/pixel). The line indicates the location of the profiles shown in Figure B3b and corresponds with the track of radar altimetry data shown in Figure B2. The image is about 46 km wide.

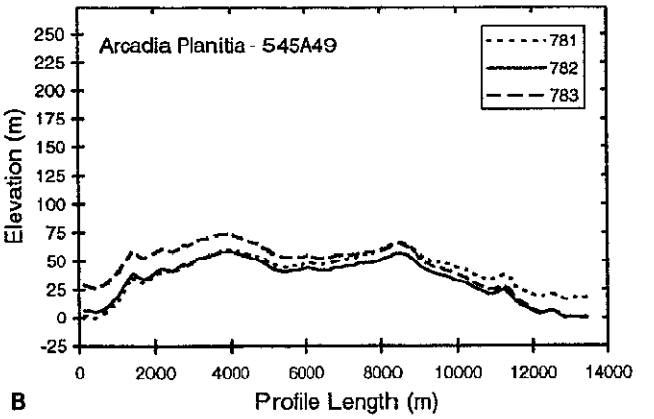

Figure B3b. Photoclinometric profiles derived using three different values of the HDN (shown in legend), holding all other parameters constant (SLV=494). Vertical exaggeration is 30:1.

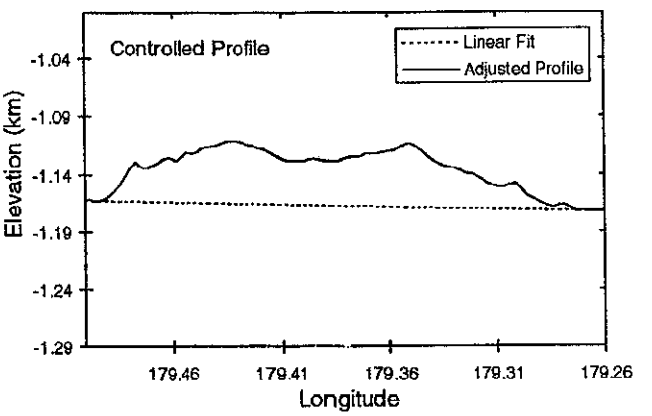

Figure B4. Controlled photoclinometric profile across a wrinkle ridge in Arcadia Planitia (20.68°N, 179.4°W). The HDN value was adjusted until the elevation difference in the photoclinometric profile between one side of the ridge and the other matched the elevation difference in corresponding points in the linear fit to the radar altimetry (see Figure B2) (HDN=782.2). Next, this adjusted profile was tied to the 6 mbar frame of reference by adding it to the corresponding points in the linear fit to the radar altimetry. Dotted line is the linear fit to the radar altimetry (see Figure B2). Elevation is relative to the 6 mbar surface, and the vertical exaggeration is 30:1. Profile was obtained in the same location as in Figure B3a.

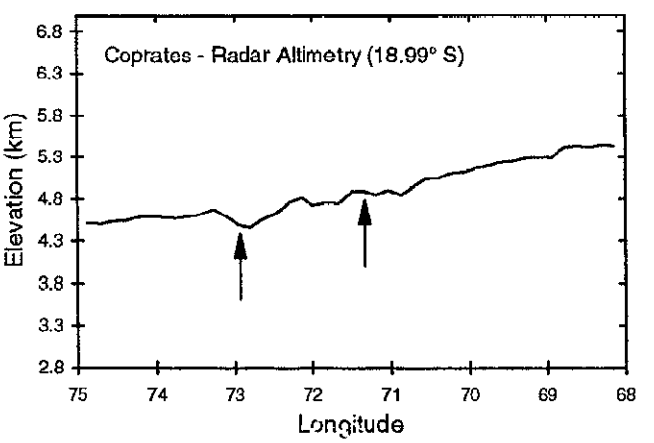

Figure B5. Earth-based radar altimetry profile across Coprates. The profile is located at 18.99°S and was derived from Goldstone radar data acquired in 1973. A westward dipping regional slope is reflected in the altimetry data. Arrows indicate the location of the profile shown in Figure B6. Altimetry is relative to the 6 mbar surface, and the vertical exaggeration is 60:1.

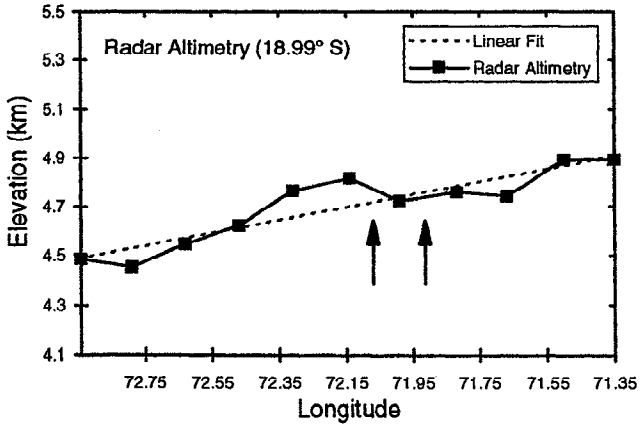

Figure B6. Goldstone radar altimetry data crossing a wrinkle ridge in Coprates (18.99°S, 72.0°W). The regional slope is defined by a linear least squares fit to the radar altimetry (m= -0.26; b=23.63). Arrows indicate the location of profiles shown in Figures B7 and B8. Altimetry is relative to the 6 mbar surface, and the vertical exaggeration is 15:1.

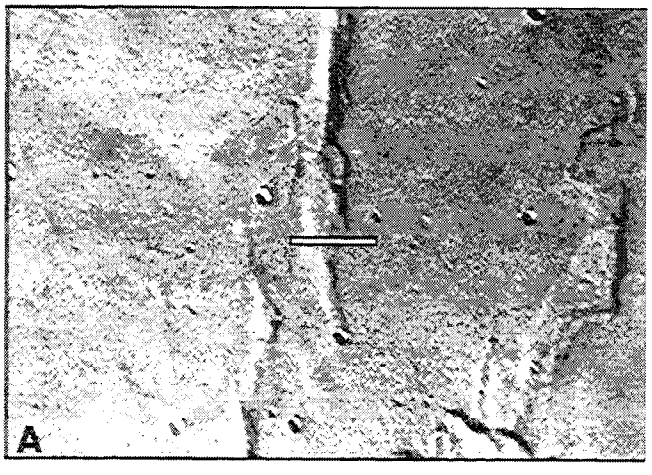

Figure B7a. Wrinkle ridge in Coprates (18.99°S, 72.0°W). Viking Orbiter image 608A49 (image resolution 217 m/pixel). The line indicates the location of the profiles shown in Figure B7b and corresponds with the track of radar altimetry data shown in Figure B6. The image is about 58 km wide.

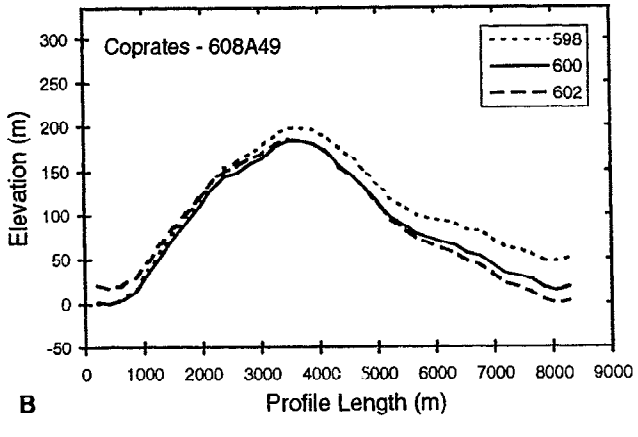

Figure B7b. Photoclinometric profiles derived using three different values of the HDN (shown in legend), holding all other parameters constant (SLV=353). Vertical exaggeration is 15:1.

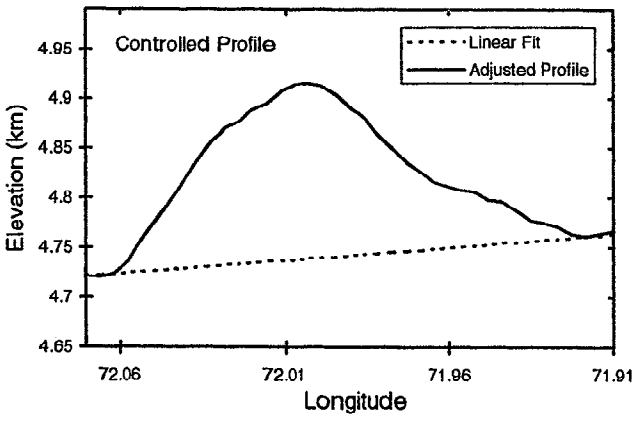

Figure B8. Controlled photoclinometric profile across a wrinkle ridge in Coprates (18.99°S, 72.0°W). The HDN value was adjusted until the elevation difference in the photoclinometric profile between one side of the ridge and the other matched the elevation difference in corresponding points in the linear fit to the radar altimetry (see Figure B6) (HDN=598.35). Next, this adjusted profile was tied to the 6 mbar frame of reference by adding it to the corresponding points in the linear fit to the radar altimetry. Dotted line is the linear fit to the radar altimetry (see Figure B6). Elevation is relative to the 6 mbar surface, and the vertical exaggeration is 15:1. Profile was obtained in the same location as in Figure B7a.

Acknowledgments. We thank Richard A. Schultz for his valuable review of the manuscript, Martin A. Slade for providing the radar altimetry data and for guidance in its interpretation and use, and Bruce A. Campbell for many useful discussions on Earth-based radar altimetry. We also thank Philip A. Davis and James R. Zimbelman for their reviews of the manuscript, and Michael J. Tuttle for his help in preparing the figures. This research was supported by grants from the National Aeronautics and Space Administration's Planetary Geology and Geophysics Program.

References

Anderson, E.M., *The dynamics of faulting and dyke formation, with applications to Britain*, 2nd ed., 206 pp., Oliver and Boyd, Edinburgh, 1951.

Anderson, J.L., The structural geology and ages of deformation of a portion of the southwest Columbia Plateau, Washington and Oregon, Ph.D. dissertation, 283 pp., Univ. of S. Calif., Los Angeles, 1987.

Binder, A.B., and J.C. Jones, Spectrophotometric studies of the photometric function, composition, and distribution of the surface materials of Mars, *J. Geophys. Res., 77*, 3005-3020, 1972.

Blasius, K.R., J.A. Cutts, and A.D. Howard, Topography and stratigraphy of the martian polar layered deposits, *Icarus, 50*, 139-159, 1982.

Bryan, W.B., Wrinkle-ridges as deformed surface crust on ponded mare lava, *Geochim. Cosmochim. Acta, 1*, suppl., 93-106, 1973.

Campbell, N.P., Structural and stratigraphic interpretation of rocks under the Yakima Fold Belt, Columbia Basin, based on recent surface mapping and well data, in *Volcanism and Tectonism in the Columbia River Flood-Basalt Province*, edited by S.P. Reidel and P.R. Hooper, *Geol. Soc. Am. Spec. Pap., 238*, 209-222, 1989.

Crosson, R.S., Small earthquakes, structure, and tectonics of the Puget Sound region (Washington), *Bull. Seismol. Soc. Am., 62*, 1133-1171, 1972.

Dahlstrom, C.D.A., Balanced cross sections, *Can. J. Earth Sci., 6*, 743-757, 1969.

Davis, P.A., and L.A. Soderblom, Modeling crater topography and albedo from monoscopic Viking Orbiter images, *Icarus*, 89, 9449-9457, 1984.

Downs, G.S., P.J. Mouginis-Mark, S.H. Zisk, and T.W. Thompson, New radar derived topography for the northern hemisphere of Mars, *J. Geophys. Res., 87*, 9747-9754, 1982.

Golombek, M.P., J.B. Plescia, and B.J. Franklin, Faulting and folding in the formation of planetary wrinkle ridges, *Proc. Lunar Planet. Sci. Conf., 21st*, 679-693, 1991.

Greeley, R., and J.E. Guest, Geologic map of the eastern equatorial region of Mars, scale 1:15,000,000, *U.S. Geol. Surv. Misc. Invest. Ser. Map, I-1802-B*, 1987.

Herkenhoff, K.E., and B.C. Murray, Color and albedo of the south polar layered deposits on Mars, *J. Geophys. Res., 95*, 1343-1358, 1990.

Howard, K.A., and W.R. Muehlberger, Lunar thrust faults in the Taurus-Littrow region, Apollo 17 Preliminary Science Report, *NASA Spec. Publ., SP-330*, 31-32--31-25, 1973.

Howard, A.D., K.R. Blasius, and J.A. Cutts, Photoclinometric determination of the topography of the martian north polar cap, *Icarus, 50*, 245-258, 1982.

Jankowski, D.G., and S.W. Squyres, Sources of error in planetary photoclinometry, *J. Geophys. Res., 96*, 20,907-20,922, 1991.

Jarchow, C.M., R.D. Catchings, and W.J. Lutter, Large-explosion source, wide-recording aperture, seismic profiling on the Columbia Plateau, Washington, *Geophysics, 59*, 259-271, 1994.

Lucchitta, B.K., Mare ridges and related highland scarps--Results of vertical tectonism, *Geochim. et Cosmochim. Acta, 3*, suppl., 2761-2782, 1976.

Lucchitta, B.K., Topography, structure, and mare ridges in southern Mare Imbrium and northern Oceanus Procellarum, *Geochim. Cosmochim. Acta, 3*, suppl., 2691-2703, 1977.

Maxwell, T.A., and R.J. Phillips, Stratigraphic correlation of the radar-detected subsurface interface in Mare Crisium, *Geophys. Res. Lett., 5*, 811-814, 1978.

Maxwell, T.A., F. El-Baz, and S.W. Ward, Distribution, morphology, and origin of ridges and arches in Mare Serenitatis, *Geol. Soc. Am. Bull., 86*, 1273-1278, 1975.

McEwen, A.S., Photometric functions for photoclinometry and other applications, *Icarus, 92*, 298-311, 1991.

Mouginis-Mark, P.J., and M.S. Robinson, Evolution of the Olympus Mons caldera, Mars, *Bull. Volcanol., 54*, 347-360, 1992.

Muehlberger, W.R., Structural history of southeastern Mare Serenitatis and adjacent highlands, *Geochim. Cosmochim. Acta, 1*, suppl., 101-110, 1974.

Pike, R.J., and P.A. Davis, Toward a topographic model of martian craters from photoclinometry (abstract), *Lunar Planet. Sci., XV*, 194-195, 1984.

Plescia, J.B., Wrinkle ridges in Lunae Planum, Mars: Implications for shortening and strain, *Geophys. Res. Lett., 18*, 913-916, 1991.

Plescia, J.B., Wrinkle ridges of Arcadia Planitia, Mars, *J. Geophys. Res., 98*, 15,049-15,059, 1993.

Plescia, J.B., and M.P. Golombek, Origin of planetary wrinkle ridges based on the study of terrestrial analogs, *Geol. Soc. Am. Bull., 97*, 1289-1299, 1986.

Reidel, S.P., K.R. Fecht, M.C. Hagood, and T.L. Tolan, The geologic evolution of the Central Columbia Plateau, in *Volcanism and Tectonism in the Columbia River Flood-Basalt Province*, edited by S.P. Reidel and P.R. Hooper, *Spec. Pap., Geol. Soc. Am., 238*, 247-264, 1989a.

Reidel, S.P., T.L. Tolan, P.R. Hooper, K.R. Fecht, M.H. Beeson, R.D. Bentley, and J.L. Anderson, The Grande Ronde Basalt, Columbia River Basalt Group: Stratigraphic descriptions and correlations in Washington, Oregon, and Idaho, in *Volcanism and Tectonism in the Columbia River Flood-Basalt Province*, edited by S.P. Reidel and P.R. Hooper, *Spec. Pap. Geol. Soc. Am., 238*, 21-53, 1989b.

Robinson, M.S., Some aspects of martian topography, Master's thesis, 75 pp., Univ. of Hawaii, Honolulu, 1991.

Roth, L.E., G.S. Downs, and R.S. Saunders, Radar altimetry of south Tharsis, Mars, *Icarus, 42*, 287-316, 1980.

Saltus, R.W., Upper crustal structure beneath the Columbia River Basalt Group, Washington: Gravity interpretation controlled by borehole and seismic studies, *Geol. Soc. Am. Bull., 105*, 1247-1259, 1993.

Schultz, R.A., Strike-slip faulting of ridged plains near Valles Marineris, Mars, *Nature, 341*, 424-426, 1989.

Schultz, R.A., and T.R. Watters, Elastic buckling of fractured basalts on the Columbia Plateau, Washington State, in *Rock Mechanics: Proceedings of the 35th U.S. Symposium*, edited by J.J.K. Daemen and R.A. Schultz, pp. 855-860, 1995.

Scott, D.H., and K.L. Tanaka, Geologic map of the western equatorial region of Mars, scale 1:15,000,000, *U.S. Geol. Surv. Misc. Invest. Ser. Map, I-1802-A*, 1986.

Sharpton, V.L., and J.W. Head, Stratigraphy and structural evolution of southern Mare Serenitatis: A reinterpretation based on Apollo Lunar Sounder Experiment data, *J. Geophys. Res., 87*, 10,983-10,998, 1982.

Sharpton, V.L., and J.W. Head, Lunar mare ridges: Analysis of ridge-crater intersections and implications for the tectonic origin of mare ridges, *Proc. Lunar Planet. Sci. Conf., 18th*, 307-317, 1988.

Simpson, R.A., J.K. Harmon, S.H. Zisk, T.W. Thompson, and D.O. Muhleman, Radar determination of Mars surface properties, in *Mars*, edited by H. Kieffer, B. Jakosky, C. Snyder, and M. Matthews, pp. 652-685, Univ. of Ariz. Press, Tucson, 1993.

Tanaka, K.L., and P.A. Davis, Tectonic history of the Syria Planum province of Mars, *J. Geophys. Res.*, 93, 14893-14907, 1988.

Tanaka, K.L., M.P. Golombek, and W.B. Banerdt, Reconciliation of stress and structural histories of the Tharsis region of Mars, *J. Geophys. Res., 96*, 15,617-15,633, 1991.

Thorpe, T.E., Mariner 9 photometric observations of Mars from November 1971 through March 1972, *Icarus, 20*, 482-489, 1973.

U.S. Geological Survey, *Planetary Image Cartography Users Manual*, Flagstaff, Ariz., 1990.

Watters, T.R., Wrinkle ridge assemblages on the terrestrial planets, *J. Geophys. Res., 93*, 10,236-10,254, 1988.

Watters, T.R., Periodically spaced anticlines of the Columbia Plateau, in *Volcanism and Tectonism in the Columbia River Flood-Basalt Province*, edited by S.P. Reidel and P.R. Hooper, *Spec. Pap. Geol. Soc. Am., 238*, 283-292, 1989.

Watters, T.R., Origin of periodically spaced wrinkle ridges on the Tharsis plateau of Mars, *J. Geophys. Res., 96*, 15,599-15,616, 1991.

Watters, T.R., A system of tectonic features common to Earth, Mars and Venus, *Geology, 20*, 609-612, 1992.

Watters, T.R., Compressional tectonism on Mars, *J. Geophys. Res., 98*, 17,049-17,060, 1993.

Watters, T.R., and R.A. Schultz, Rock mass strength criterion applied to ridge plains on Mars: Implications for elastic buckling, *Proc. Lunar Planet. Sci. Conf., 26th*, 1471-1472, 1995.

Wildey, R.L., Generalized photoclinometry for Mariner 9, *Icarus, 25*, 613-626, 1975.

Zuber, M.T., and L.L. Aist, The shallow structure of the martian lithosphere in the vicinity of the ridged plains, *J. Geophys. Res., 95*, 14,215-14,230, 1990.

M. S. Robinson, Department of Geological Sciences, Northwestern University, Evanston, Illinois 60208.
(email: mrobinson@earth.nwu.edu)

T. R. Watters, Center for Earth and Planetary Studies, National Air and Space Museum, Smithsonian Institution, Washington, DC 20560. (email: twatters@ceps.nasm.edu)

(Received August 16, 1996; revised January 30, 1997;
accepted February 10, 1997.)